

Molecular Recognition of Sub-micromolar Inhibitors by the Epinephrine-Synthesizing Enzyme Phenylethanolamine *N*-Methyltransferase

Fiona M. McMillan,[†] Julia Archbold,^{†,‡} Michael J. McLeish,^{§,||} Joanne M. Caine,^{§,⊥} Kevin R. Criscione,[#] Gary L. Grunewald,[#] and Jennifer L. Martin^{*,†}

Centre for Drug Design and Development and Special Research Centre for Functional and Applied Genomics, Institute for Molecular Bioscience, University of Queensland, Brisbane QLD 4072, Australia, Victorian College of Pharmacy, Monash University, Parkville VIC 3052, Australia, and Department of Medicinal Chemistry, The University of Kansas, Lawrence, Kansas 66045-7582

Received December 19, 2002

The crystal structures of human phenylethanolamine *N*-methyltransferase in complex with *S*-adenosyl-L-homocysteine (**7**, AdoHcy) and either 7-iodo-1,2,3,4-tetrahydroisoquinoline (**2**) or 8,9-dichloro-2,3,4,5-tetrahydro-1*H*-2-benzazepine (**3**, LY134046) were determined and compared with the structure of the enzyme complex with **7** and 7-aminosulfonyl-1,2,3,4-tetrahydroisoquinoline (**1**, SK&F 29661). The enzyme is able to accommodate a variety of chemically disparate functional groups on the aromatic ring of the inhibitors through adaptation of the binding pocket for this substituent and by subtle adjustments of the orientation of the inhibitors within the relatively planar binding site. In addition, the interactions formed by the amine nitrogen of all three inhibitors reinforce the hypothesis that this functional group mimics the β -hydroxyl of norepinephrine rather than the amine. These studies provide further clues for the development of improved inhibitors for use as pharmacological probes.

Introduction

Phenylethanolamine *N*-methyltransferase (PNMT, EC 2.1.1.28) catalyzes the synthesis of epinephrine (**5**) by methylation of norepinephrine (**4**) using the methyl donor *S*-adenosyl-L-methionine (**6**, AdoMet) (Figure 1). The enzyme is a 31 kDa protein expressed predominantly in the adrenal medulla, where **5** is secreted as a hormone, and in the central nervous system (CNS),^{1,2} where **5** is released as a neurotransmitter. The crystal structure of human PNMT (hPNMT) complexed with the inhibitor 7-aminosulfonyl-1,2,3,4-tetrahydroisoquinoline (**1**, SK&F 29661) and cofactor product (**7**, *S*-adenosyl-L-homocysteine, AdoHcy) was recently reported.³

We are interested in elucidating the role of central epinephrine by inhibiting CNS epinephrine biosynthesis. To do this, inhibitors of PNMT that are potent (active in the nanomolar range), selective (inactive against other adrenoceptor systems such as the α_2 -adrenoceptor), and capable of crossing the blood–brain barrier (BBB)⁴ are required. However, most of the currently available inhibitors of PNMT developed by analogue-based methods have K_i values in the micromolar, rather than the nanomolar range, or are not selective because they interact with the catecholamine α_2 -adrenoceptor at concentrations similar to those at which they inhibit PNMT.^{5,6} Inhibitors of PNMT with

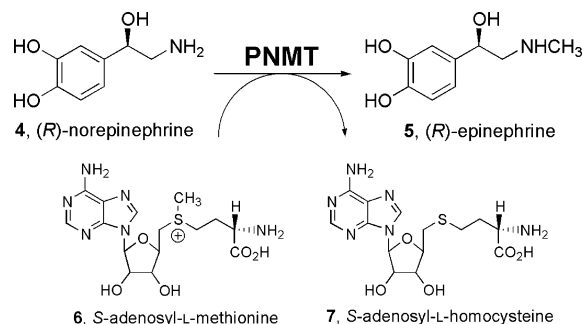


Figure 1. Schematic showing the chemical reaction catalyzed by PNMT. PNMT transfers an activated methyl group from *S*-adenosyl-L-methionine (**6**, AdoMet) to the amine of norepinephrine (**4**) to produce epinephrine (**5**) and *S*-adenosyl-L-homocysteine (**7**, AdoHcy).

improved characteristics are therefore required and will be designed by structure-based methods.

A number of current inhibitors of PNMT are based on either a tetrahydroisoquinoline (THIQ)⁷ or tetrahydrobenzazepine (THBA)⁸ framework. In this paper, the molecular recognition by PNMT of three sub-micromolar inhibitors using protein crystallography has been investigated. These are the THIQ derivatives **1** and **2** and the THBA derivative **3** (Table 1). Within this small set of inhibitors, we nonetheless have either hydrophilic (SO₂NH₂) or lipophilic (Cl, I) substituents on the aromatic ring.

The crystal structure of PNMT:7:1, that is hPNMT complexed with AdoHcy (**7**) and a relatively selective inhibitor **1** (Table 1), was recently determined.³ The 7-sulfonamide group on the THIQ moiety makes the inhibitor **1** too polar to cross the BBB⁹ [calculated log *P* (ClogP) = −0.24, Table 1] and it is therefore ineffective as a pharmacological tool for the study of CNS epinephrine. Compound **2** has an iodine at the 7-posi-

* To whom correspondence should be addressed. Phone +61 7 3346 2016. Fax +61 3346 2101. E-mail: j.martin@imb.uq.edu.au.

[†] University of Queensland.

[‡] Present address: Natural Products Discovery, Griffith University, Brisbane QLD, Australia.

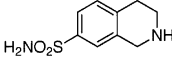
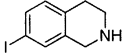
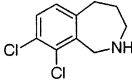
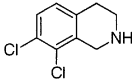
[§] Monash University.

^{||} Present address: College of Pharmacy, University of Michigan, Ann Arbor MI 48109-1065.

[⊥] Present address: CSIRO Molecular Science, Parkville, Victoria 3052 Australia.

[#] The University of Kansas.

Table 1. PNMT Inhibitor Data

Compound	(A) PNMT	(B) α_2	B/A	ClogP ^b
	$K_i \pm \text{SEM}$ (μM) ^a	$K_i \pm \text{SEM}$ (μM) ^a	Selectivity	
1 	0.56 ± 0.04	100 ± 20	180	-0.24
2 	0.37 ± 0.04	0.22 ± 0.04	0.6	2.72
3 	0.26 ± 0.03	4.5 ± 0.3	17	3.31
8 	0.22 ± 0.05	0.021 ± 0.005	0.095	2.90

^a PNMT and α_2 K_i values are taken from ref 10 for **1**, **3**, and **8** and from ref 7 for **2**. K_i values are shown for bovine PNMT, since values for human PNMT are not available. However, a comparison study has shown that inhibitor activity against the human enzyme is similar to that at the bovine enzyme (ref 34) and that the rank order of potency is the same. ^b ClogP values were calculated using the SYBYL (v. 6.9, ref 30) software package and are the calculated logarithm of the octanol–water partition coefficient, indicating the lipophilicity of the compound. A ClogP value of greater than 0.5 appears to be required to allow passage across the BBB (ref 10).

tion, and should be sufficiently lipophilic to pass the BBB.¹⁰ However, **2** is the least selective of the three inhibitors (Table 1). Compound **3**, which has chloro substituents at two adjacent positions on the aromatic ring and incorporates a seven-membered, rather than a six-membered, fused aliphatic ring, is a sub-micromolar PNMT inhibitor and its ClogP value suggests that it should cross the BBB,¹⁰ but it is much less selective for PNMT than **1** (Table 1). These three compounds were chosen for crystallization in order to (1) determine the validity of a CoMFA model, which hypothesized a different binding orientation for compounds with hydrophilic aromatic substituents versus those with lipophilic substituents,^{7,11} and (2) determine the area in space occupied by the increased steric bulk (additional methylene unit, as compared to THIQ) of the seven-membered aliphatic ring of **3**. This “pucker” in the aliphatic ring is readily accommodated by the enzyme active site and the crystal structure should illustrate how the “pucker” fits therein. While **3** is not as selective as **1** (PNMT inhibitory potency versus α_2 -adrenoceptor affinity), it is significantly more selective than its 7,8-dichloro THIQ analogue (**8**, SK&F 64139, Table 1). Thus, determining the region of space where the pucker occurs will likely explain which enantiomer of 3-substituted-THIQs should bind better at the active site of PNMT. These enantiomers of 3-substituted-THIQs may provide an additional approach to improving the selectivity of this class of inhibitors.

Using structural methods, we investigated how the enzyme accommodates the different aromatic substituents of these inhibitors. Such information will be useful for the structure-based design of modified inhibitors that are sufficiently potent, selective, and lipophilic for studies on CNS epinephrine. Crystal structures of the

two new PNMT:inhibitor complexes (PNMT:**7:2** and PNMT:**7:3**) are presented and compared with the structure of the PNMT complex with **1** (PNMT:**7:1**).

Results

Crystals of the PNMT:**7:2** and PNMT:**7:3** complexes were isomorphous with the recently determined structure of PNMT:**7:1**³ and their crystal structures were solved by difference Fourier methods (Table 2). In both new structures, the enzyme fold is the same as that described for the PNMT:**7:1** complex. The crystal structures of all three inhibitor complexes also show that the inhibitors and cofactor products are bound in equivalent sites in the enzyme in each case (Figure 2).

Enzyme Structures Are the Same. A root-mean-square deviation (rmsd) analysis of the three enzyme–inhibitor complexes (Table 3) confirms that there are no significant enzyme structural differences between the complexes. This is despite significant variations in the resolution of the diffraction data (2.4–2.8 Å) and the structural differences of the inhibitors. The data in Table 3 imply that there are greater differences in the structures of the two monomers in one asymmetric unit (0.50–0.55 Å rmsd) than there are between the enzymes complexed with different inhibitors (0.24–0.33 Å rmsd). Crystal contacts are largely responsible for structural differences between monomers A and B, and these are localized to specific surface regions. For example, the structure of the surface loop linking αB and α4 (residues 111–119) differs by >3 Å rmsd between the two monomers. In monomer A, this loop forms no crystal contacts, while in monomer B it makes several interactions with α2 , the ω -loop, and the β -hairpin of a symmetry-related monomer A. This induces a change

Table 2. X-ray Data and Refinement Statistics for Two PNMT Inhibitor Complexes

	PNMT:7:2	PNMT:7:3
Data Measurement		
space group	$P4_32_12$	$P4_32_12$
unit cell (Å)		
<i>a</i> , <i>b</i>	94.7	94.4
<i>c</i>	186.9	186.6
α , β , γ	90°, 90°, 90°	90°, 90°, 90°
observations	52 232	80 055
unique reflections	22 078	20 430
resoln range (Å) (top shell)	50–2.7 (2.8–2.7)	50–2.8 (2.9–2.8)
$I/\sigma(I)$	13.6 (2.1)	14.4 (2.5)
completeness ^a (%)	91.3 (77.0)	94.7 (89.0)
R_{merge}^b (%)	7.5 (27.9)	7.5 (33.2)
Refinement		
resolution range (Å)	50–2.7	50–2.8
reflns ($ F > 0$) of working set (test set)	19 883 (2192)	18 408 (2008)
$R_{\text{cryst}}^c/R_{\text{free}}^d$ (%)	23.2/26.8	22.6/27.8
no. non-hydrogen atoms		
protein and ligands	4139	4141
water	56	32
rmsd from ideal geometry		
bond length (Å)	0.008	0.010
bond angle (deg)	1.40	1.54
Ramachandran (nonglycine)		
% in most favored region	90.6	87.9
% in disallowed region	0.2	0.0

^a Completeness indicates the number of measured independent reflections divided by the total theoretical number of independent reflections. ^b $R_{\text{merge}} = \sum |I_{\text{obs}} - I_{\text{av}}| / \sum I_{\text{av}}$, over all symmetry-related observations. ^c $R_{\text{cryst}} = \sum |F_{\text{obs}} - F_{\text{calc}}| / \sum |F_{\text{obs}}|$, over all reflections. ^d R_{free} (ref 29) is calculated as for R_{cryst} from 10% of the data excluded from refinement. ^e Engh and Huber parameters were used in refinement (ref 35).

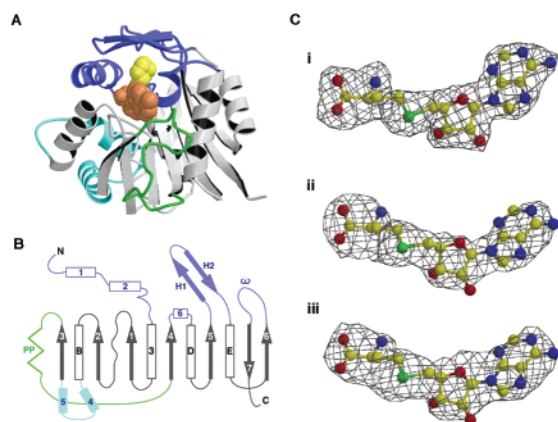


Figure 2. (A) A ribbon diagram of the PNMT:7:3 structure, showing **7** (orange) and **3** (yellow) bound in the active site. (B) A diagram of the secondary structure of PNMT. In both panels A and B, secondary structural elements that make up the core fold are in gray and white. Colors indicate large insertions: blue for the active-site cover, green for the polyproline linker region, and cyan for the 2-helix C-terminal insertion. (C) An $F_o - F_c$ OMIT map for **7** from the structures of PNMT bound with (i) **1** (ii) **2**, and (iii) **3**.

in the monomer B loop structure compared to the noncrystallographically related monomer A loop. Other regions that vary between monomers A and B are at the N-terminus (to residue 28), helix $\alpha 5$ (residues 141–149), the polyproline region (residues 165–172), the loop following αD (residues 207–209), the β -hairpin (residues 223–232), and the loop following αE (residues 249–252). When these are excluded from the calculation, the average rmsd for comparison of monomers A and B is

Table 3. Root-Mean-Square Deviation (Å) for C_α Atom Superimposition of Subunits A, B or A and B in the Three PNMT:Inhibitor Crystal Structure Complexes (**1**, **2**, and **3**)

PNMT subunits within the same crystal structure (A vs B)	1 (A)	2 (A)	3 (A)
1 (B)	0.50	–	–
2 (B)	–	0.53	–
3 (B)	–	–	0.55
Same subunit in three different crystal structures (A vs A)			
1 (A)	–	0.30	0.31
2 (A)	–	–	0.24
Same subunit in three different crystal structures (B vs B)			
1 (B)	–	0.29	0.29
2 (B)	–	–	0.21
Two subunits (A and B) in three different crystal structures			
1 (A & B)	–	0.31	0.33
2 (A & B)	–	–	0.24

0.33 Å, similar to that for comparison of two PNMT structures complexed with different inhibitors.

Cofactor Binding. Electron density for the cofactor product (**7**) is clear and unambiguous in both the PNMT:7:2 and the PNMT:7:3 structures. The density for **7** in each of the complexes (Figure 2C) indicates that the binding orientation, conformation, and enzyme interactions of the cofactor product in the two new structures are the same as that in the PNMT:7:1 structure. The enzyme side-chain positions in the cofactor-binding site are also unchanged. Given that the cofactor-binding sites are similar and that the rmsd analysis indicates that there is no change in the overall structure of the enzyme upon binding the three inhibitors, the structural basis for variation in the binding of the compounds must be localized to the substrate/inhibitor-binding site.

7-Aminosulfonyl-1,2,3,4-tetrahydroisoquinoline (1). To analyze and compare the binding modes of the three inhibitors, we begin with the enzyme complex formed with **1**.³ The refined OMIT electron density for the inhibitor is shown in Figure 3A. Significant interactions between **1** and the enzyme are summarized in Figure 4A and described as follows. The aromatic ring is sandwiched between the side chains of Phe182 and Asn39 (Figure 5B). The aliphatic amine forms a hydrogen bond to Glu219 and water-mediated hydrogen bonds to the side chains of Asp267 and Asn39 (not shown). The amine is also within 4.1 Å of the aromatic ring of Tyr222, suggesting a weak amino–aromatic interaction. The closest distance between the sulfur of **7** and the inhibitor is 5.4 Å to the aliphatic C4 methylene and the distance between the sulfur of **7** and the inhibitor amine is 7.3 Å (for both monomers). Both sulfonamide oxygens can interact with the side chain amine of Lys57, and one of these also makes water-mediated interactions with the main chain of Arg44 and the side chain of Tyr126 (not shown). The sulfonamide nitrogen is within 3.5 Å of both the *S*-methyl of Met258 and the guanidino group of Arg44 (not shown), although the latter is involved in an ion pair interaction with Asp267. The sulfonamide nitrogen thus does not appear to form any favorable interactions with the enzyme, which confirms previous SAR studies.¹²

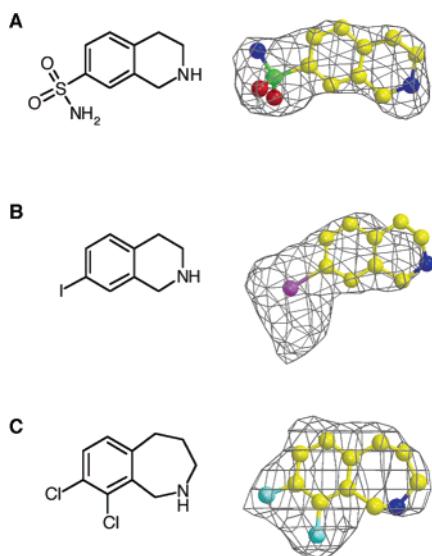


Figure 3. Chemical structures of the three inhibitors are shown beside their refined PNMT-bound conformations taken from the three crystal structures: (A) **1**, (B) **2** and (C) **3**. The OMIT calculated $F_o - F_c$ electron density maps for the three inhibitors are also shown. These were calculated using the final refined model of the enzyme complex, with the inhibitor omitted from the map calculation. The electron density around the iodo substituent of **2** in (B) is continuous with that of Met258 (not shown) and is consistent with the scattering expected from an atom of this size. Although partial disorder is observed around the aliphatic ring of **2**, the binding mode for the inhibitor is established by the strong density for the iodine and aromatic ring (see Experimental Section).

7-Iodo-1,2,3,4-tetrahydroisoquinoline (2). The OMIT electron density map is consistent with the chemical structure of **2**, showing strong density for the 7-iodo-substituent, but weaker density for the aliphatic ring (Figure 3B). The halogen substituent interacts with Val53 (3.5 Å) and Met258 (2.6 Å) (Figure 4B). The latter interaction appears to be quite strong, as indicated by an extension of the electron density downward (Figure 3B) from the iodo substituent and toward Met258. The bound conformation of **2** is essentially planar, with a slight puckering of the aliphatic six-membered ring at C3 (Figure 5). As observed for the complex with **1**, the aromatic ring of **2** is sandwiched between Phe182 (3.8 Å) and Asn39 (3.5 Å) (Figure 5B). The aliphatic amine forms a hydrogen bond to the carboxylate of Glu219 (3.0 Å) and is 3.4 Å from the ring of Tyr222, suggesting a strong amino–aromatic interaction (Figure 4B). The amine is also involved in a water-mediated hydrogen bond to Asp267 (Figure 5B), similar to that in the complex with **1**. The 7-iodo group binds in a small hydrophobic pocket bounded by side chains from Met258, Val53, Val269, and Val272 (last not shown). The closest charged group to the 7-iodo is Arg44 (4.2 Å); however, as noted previously this side chain forms an ion pair with Asp267, so the charge may not be apparent. Once again there is no direct interaction between the inhibitor and the cofactor, although **2** makes the closest approach to **7** of the three inhibitors described here (4.6 Å from the sulfur of **7** to the C4 methylene of **2**). The distance between the sulfur of **7** and the aliphatic amine of **2** is 6.3 Å.

8,9-Dichloro-2,3,4,5-tetrahydro-1H-2-benzazepine (3). The refined OMIT electron density for **3** in

the substrate-binding site is consistent with the inhibitor chemical structure (Figure 3C), showing bulges for the 8- and 9-chloro substituents and puckering of the seven-membered aliphatic ring. As in the complexes with **1** and **2**, the aromatic ring is sandwiched between Phe182 and Asn39 (Figure 5B). The closest distance between **3** and the sulfur of **7** is 5.4 Å (Figure 4C) to the C5 methylene of the aliphatic ring. The distance between the sulfur of **7** and the aliphatic amine is 7.9 Å. Several hydrogen bonds are formed between the amine of **3** and the enzyme; the large pucker in the seven-membered aliphatic ring allows the amine to form direct interactions with both Glu219 (3.2 Å) and Asp267 (2.7 Å), in contrast to the water-mediated interactions observed for interaction with Asp267 in the complexes with **1** and **2**. This water is not observed in the complex with **3** and is apparently displaced by the inhibitor amine (Figure 5B). However, the puckered ring conformation of **3** places the amine 4.9 Å from the aromatic ring of Tyr222 (as compared with 4.1 Å for **1** or 3.4 Å for **2**), so **3** is unlikely to have a significant amino–aromatic interaction in contrast to the other two inhibitors. Additional interactions between **3** and the enzyme are, for the most part, van der Waals (Figure 4C). The 8-chloro substituent interacts with Val53 (3.4 Å) and the side chain amine of Lys57 (3.7 Å), and the 9-chloro substituent interacts with Met258 (2.5 Å) (Figure 5A).

Comparison of Inhibitor Binding. We compared the binding modes for each of the three inhibitor-bound structures of PNMT by superimposing the enzyme structures. All three inhibitors occupy the same region of space (Figure 5), sandwiched between Phe182 and Asn39, and all three are oriented in the same way with the aromatic ring substituent closest to the N-terminus of α -helix 3 of the enzyme fold and the aliphatic amine closest to H1 of the β -hairpin forming part of the cover of the active site³ (Figure 2B).

Discussion

There are significant differences in the binding mode of these three inhibitors. Although **1** and **2** both incorporate the same THIQ ring system, their THIQ scaffolds do not superimpose. The THIQ moiety of **2** is translated in the binding site by ~ 1.2 Å relative to **1** and by ~ 0.8 Å relative to **3** (Figure 5A) and, furthermore, the fused ring system is rotated by $\sim 15^\circ$ around the planar axis in the active site relative to the other two inhibitors. This translation and rotation of the inhibitor scaffold of **2** is apparently due to the presence of the 7-iodo substituent. As a consequence of the translation and rotation, the aliphatic amine of **2** is located in a different position than that of **1** in the active site, although the amine makes similar interactions with the enzyme in both cases. Our previous QSAR and CoMFA analysis of these two compounds predicted that they would bind differently to the enzyme, and we proposed a model to explain this whereby the ligand could bind to the enzyme in one of two different orientations, depending on the lipophilicity of the 7-substituent (Figure 6).⁷ The previous model also proposed that although the amines would be located differently in the active site, they would make similar interactions with the enzyme, albeit from different directions. The crystal structures in this study show that this simplistic hypothesis regarding the

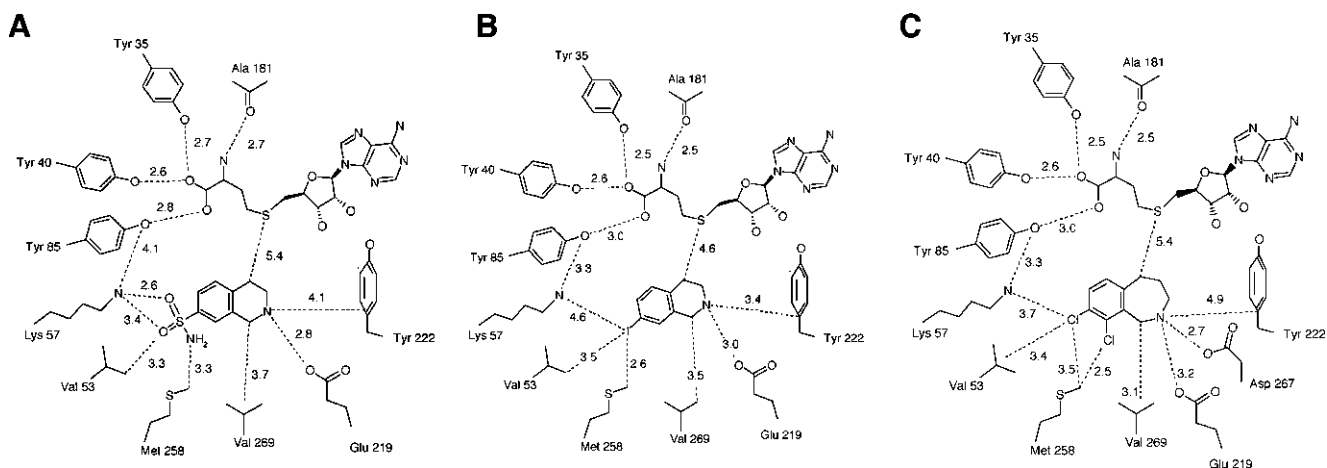


Figure 4. Schematics showing important interactions formed between the inhibitors and PNMT at the active site; dashed lines indicate distances in angstroms: (A) **1**, (B) **2**, (C) **3**. For clarity, some interactions mentioned in the text are not shown. The closest distance formed between each of the inhibitors and the sulfur of **7** is also shown.

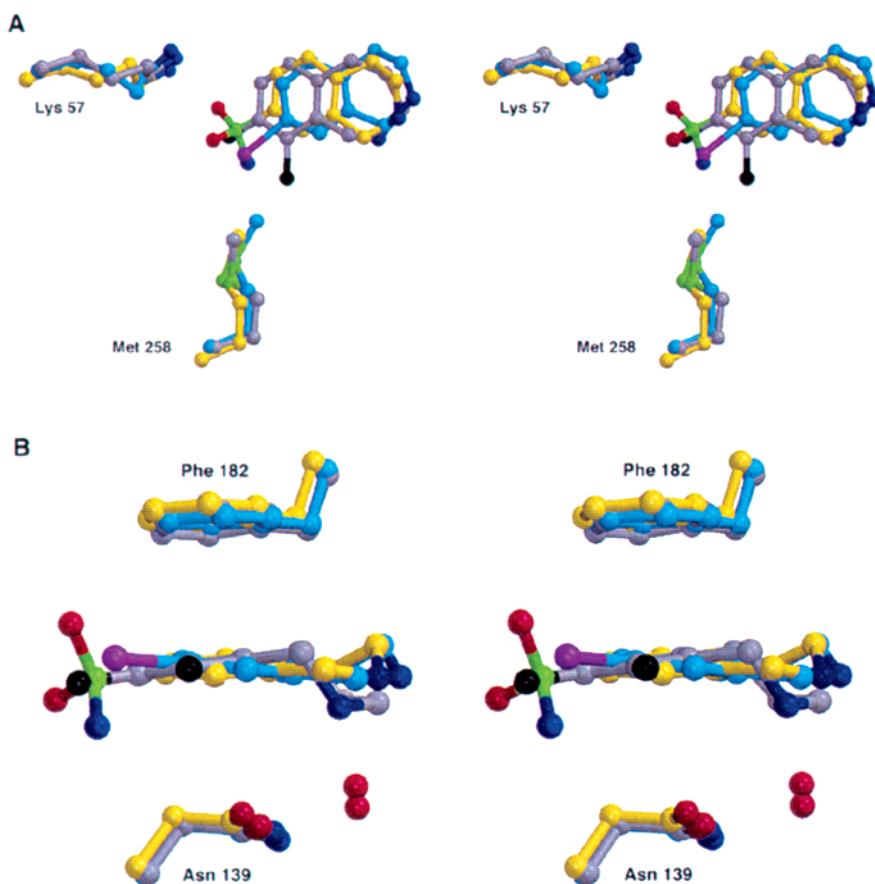


Figure 5. Comparison of inhibitor binding to PNMT. (A) Stereodiagram of the binding mode of the three inhibitors after superimposition of the enzyme structures, also showing the relative orientations of active site residues Lys57 and Met258 in the active site of PNMT. Atoms corresponding to **1** are shown in yellow, **2** in light blue (iodine in pink), and **3** in gray (chlorines in black). Oxygen atoms are shown in red, nitrogens in blue, and sulfurs in green. (B) A side view of the same superimposition. Residues Asn39 and Phe182 from PNMT form a narrow planar cleft within the enzyme active site. The amine-interacting water from the cocrystal structures with **1** and **2** are shown. This water is displaced by the out-of-plane amine of **3**.

binding of the inhibitors to the active site of PNMT to be incorrect and that it is changes in the amino acid positions in the enzyme active site that occur to accommodate the two classes (hydrophilic versus lipophilic aromatic substituents) of inhibitor.

The crystal structures also show that the binding mode of **3** is more like that of **1** than that of **2**, even though **3** incorporates a lipophilic halogen substituent rather than a hydrophilic substituent like **1**. Thus, the

aromatic ring moieties of **1** and **3** adopt a similar bound position and orientation in the enzyme, although **3** is translated by ~ 0.4 Å away from the 7-substituent binding pocket compared with **1**, presumably to accommodate the two chloro substituents on the aromatic ring. Curiously, the 8-chloro substituent of **3** and the sulfur atom of the sulfonamide of **1** are almost coincident (Figure 5). How is it that these very different chemical substituents can bind in the same pocket of the enzyme?

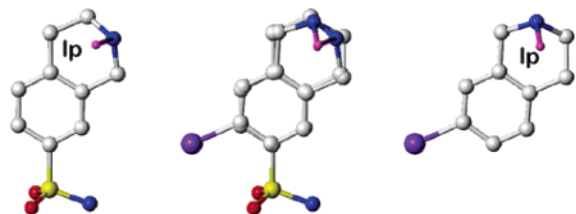


Figure 6. Structures of the proposed orientations of **1** (hydrophilic 7-substituent, left structure) and **2** (lipophilic 7-substituent, right structure) from the CoMFA model (ref 7, 11), showing how the 7-substituents would be in different areas of space, depending on the lipophilicity of the substituent. The center structure is a superimposition of **1** and **2**, which shows that the lone pairs (lp) on the aliphatic ring nitrogens can reach the same area, albeit from different directions. This model, which suggested a 180° flip of the THIQ nucleus depending on the lipophilicity of the 7-substituent, is clearly invalidated by the present study. However, the model is correct insofar as it predicted that the same amino acid residue(s) could interact with the THIQ amine functionality.

It appears that the pocket can adopt a variable hydrophobic nature depending on the substituent in this position. The major changes occur at residues Lys57 and Met258. Lys57 forms the majority of direct hydrogen bonds with the sulfonamide oxygens of **1**, but shifts away from the binding pocket by up to 1 Å when the iodo substituent of **2** or the 8-chloro substituent of **3** are present. In these two structures, the Lys57 side chain forms a hydrogen bond with the side chain of Tyr85, an interaction that is not observed in the structure of PNMT complexed with **1** (Figure 4). Furthermore, the Met258 side chain also appears to be mobile in the binding pocket, moving by up to 2 Å toward the halogen substituents of **2** and **3** and away from the sulfonamide of **1**. The sulfonamide oxygen of **1** forms a water-mediated (3.0 Å) hydrogen bond with the main chain of Arg44. It is not clear whether a similar water is present in this region is poor, although any such interactions would presumably be weaker than those observed in the complex with **1**. However, this may be compensated for by a strong interaction between the 8-chloro of **3** and the guanidino group of Arg44 (3.0 Å).

Unfortunately, the crystal structures in this study do not provide sufficient information to allow the unambiguous determination of how a 3-substituent on THIQ may overlap with the additional methylene unit ("pucker") in the aliphatic ring of **3**. While SAR studies have shown a stereochemical preference^{13,14} and molecular modeling studies have shown how this could occur (Figure 7), it will require the cocrystallization of hPNMT with a 3-substituted-THIQ or a THBA with similar aromatic substituents to answer this question.

The PNMT inhibitors **1–3** each incorporate three chemical features: a fused ring system, an aliphatic amine, and an aromatic ring substituent. The aromatic ring system appears to be the most crucial element for binding to PNMT, allowing inhibitors to slot into the narrow binding cleft between the side chains of Phe182 and Asn39 at the active site (Figure 5). The next most important feature appears to be the aromatic ring substituent, which alters the inhibitor binding mode, although not in the simplistic manner as previously hypothesized (Figure 6).⁷ The model we proposed to explain the different binding modes must now be

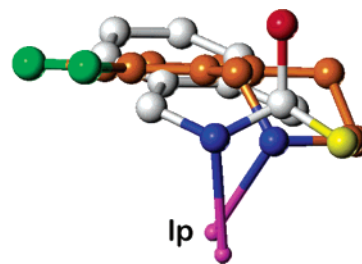


Figure 7. Overlay of **3** (from the crystal structure, shown in orange) and 3,3-dimethyl-THIQ (shown in white), showing that the pucker of the seven-membered ring of **3** and a 3*S*-methyl on THIQ (shown in yellow) are close to the same area in space, while a 3*R*-methyl (shown in red) would be in a different area in space.

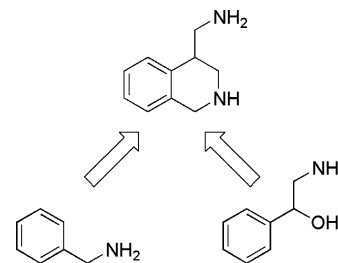


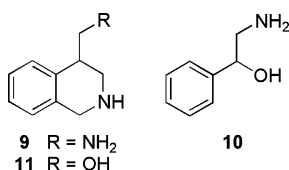
Figure 8. Hypothetical binding orientations for benzylamine inhibitors and phenylethanolamine substrates. This model suggests that the benzylamine nitrogen occupies a similar binding region at the active site of PNMT as does the β -hydroxyl of phenylethanolamines. Confirmation of the model is the observation that 4-aminomethyl-THIQ (**9**) is a better substrate than is phenylethanolamine (**10**) (ref 15). The observation in this paper that the distances from the AdoHcy (**7**) sulfur to the aliphatic amine of **1–3** is 6–8 Å implies that this nitrogen is not binding where the nitrogen of phenylethanolamine substrates would bind but rather is close to the region where the β -hydroxyl binds. The present study lends strong support to this model (see text).

revised. Rather than two alternate binding pockets in the enzyme for 7-substituents (one lipophilic, one hydrophilic) there is only one pocket that has the capacity to accept either lipophilic or hydrophilic substituents. Thus, the substituents of all three inhibitors bind in close proximity to each other in the active site, with the *enzyme* adapting its chemistry to accommodate the different substituent chemistries presented. However, the size of the substituent does affect the precise positioning and orientation of the inhibitor framework, causing significant translation and rotation of the inhibitor molecule in the binding site, as in the case of **2**.

The aliphatic amine is the most adaptable binding feature of the inhibitors, with a separation of ~1–2 Å for any two of the amines of the three superimposed inhibitors in the active site (Figure 5). Yet in all three cases, the amine makes several energetically favorable interactions with the same enzyme residues. Thus, the enzyme accepts alternate presentations of the amine, allowing similar interactions to form in all three cases. This result provides support for our hypothesis that the amines of inhibitors of PNMT can bind in different positions in the active site while still interacting with common enzyme residues.⁷

The natural substrate of PNMT, norepinephrine (**4**), incorporates an aromatic ring and an amine as well as a hydroxyl group that is critical for its substrate specificity. The inhibitors **1–3** each incorporate an

aromatic ring and an amine, and potentially act as conformationally restricted analogues of **4**. The reaction catalyzed by PNMT requires nucleophilic attack by the amine nitrogen of **4** on the methyl group of the cofactor. For such an attack to occur, the amino group must approach to within 2–3 Å of the AdoMet (**6**) methyl carbon and, by extrapolation, to within 4–5 Å of the sulfur of **6** or **7**. However, the ring nitrogens of **1**, **2**, and **3** are located 7.3, 6.3, and 7.9 Å, respectively, from the sulfur of **7**. This is further confirmation of previous SAR studies that suggested that the amine moieties of these inhibitors do not mimic the amine of **4** but, more likely, mimic the β -hydroxyl group (Figure 8).¹⁵ These conclusions were based on the observations that 4-amino-methyl-1,2,3,4-tetrahydroisoquinoline (**9**, $K_m = 47 \pm 9 \mu\text{M}$, $V_{\text{max}} = 3.4 \pm 0.3 \text{ nmol/min/mg}$) was a better substrate for PNMT than phenylethanolamine (**10**, $K_m = 70 \pm 6 \mu\text{M}$, $V_{\text{max}} = 2.2 \pm 0.2 \text{ nmol/min/mg}$), and that 4-hydroxymethyl-1,2,3,4-tetrahydroisoquinoline, although it bound to the enzyme (**11**, $K_i = 170 \pm 10 \mu\text{M}$), was not a substrate.



Analysis and comparison of the three PNMT inhibitor complexes has enabled us to identify critical chemical components for PNMT binding and inhibition. We intend to further investigate PNMT inhibition to achieve our goal of clarifying the precise physiological role of CNS epinephrine by inhibiting its biosynthesis *in vivo*. Although current inhibitors are not appropriate for this task, they have proven to be enormously useful for mapping the PNMT pharmacophore. This information will be useful in future inhibitor design studies, the results of which may be used to develop pharmacological tools aimed at clarifying the proposed roles of CNS epinephrine in the central control of blood pressure,¹⁶ respiration,¹⁷ and pituitary hormone secretion¹⁸ and to investigate further the link between CNS epinephrine and ethanol intoxication¹⁹ or Alzheimer's disease.²⁰

Experimental Section

Crystallization of PNMT–Inhibitor Complexes. Recombinant wild-type human PNMT was produced as described previously.²¹ Compound **1** was kindly provided by Smith Kline and French Laboratories, Smith Kline Beecham Corp., Philadelphia, PA. Compounds **2** and **3**²² were synthesized as described previously. Protein crystallization was performed using the method described to produce crystals of the PNMT:7:1 complex.²³ Protein homogeneity was assessed by SDS–PAGE and purified PNMT was concentrated to >100 mg/mL in 20 mM Tris buffer, pH 7.2, 1 mM EDTA, and 0.5 mM DTT. DTT, cofactor product, and inhibitor were added to the following concentrations: 11 mM DTT, 2 mM **7**, and 11 mM **2** or 15 mM **3**. The final concentration of protein was 80 mg/mL. Complexes were crystallized at 20 °C by hanging drop vapor diffusion in cacodylate buffer (0.1 M, pH 6–6.25) using PEG 6K (6–10%) and lithium chloride (0.25 M) as precipitant. Crystal complexes with either **2** or **3** grew within 3–4 weeks. Crystals were isomorphous with PNMT:7:1 crystals, with space group $P4_32_12$ and two monomers in the asymmetric unit. Crystals of the complex with **2** or **3** were soaked in cryo-

protectant-containing reservoir solution plus 25% glycerol and then flash frozen in a gaseous nitrogen stream (100 K).

Data Measurement and Structure Determination. Diffraction data for the two crystals were measured using a Rigaku RU200HR copper rotating anode generator (operating at 46 kV and 60 mA) with a Yale Mirror system. An Oxford cryostream and an RAXIS-IIC image plate area detector were used for data measurement at 100 K. Crystallographic statistics for the single-crystal data from both complexes are summarized in Table 2.

Crystallographic data were processed using DENZO and SCALEPACK²⁴ and phasing was carried out using CNS v0.9.²⁵ The PNMT:7:2 complex (PDB code 1N7J) was solved by difference Fourier methods using the structure of PNMT:7:1 as the model (PDB code 1HNN).³ The PNMT:7:3 structure (PDB code 1N7I) was solved by difference Fourier methods using the refined structure of the PNMT complex with **7** and **2**. Model building was performed using O,²⁶ and the structures were refined using CNS v0.9.²⁵ Initial coordinates for the inhibitors were generated using Insight II.²⁷ Topology and parameter files were generated for the two inhibitors using XPLO2D²⁸ and modified where necessary. The procedure used was to model the structure of the protein first and then add water molecules, followed by **7** and finally the inhibitor. R -free analysis (10% of reflections) was used for cross-validation.^{25,29}

Structural Analysis. The final models for both enzyme–inhibitor complexes comprise 261 of 282 residues in one monomer of the asymmetric unit and 267 of 282 residues in the other. The missing residues are at the N-terminus in each case; electron density was not observed for residues 1–21 in the first monomer and residues 1–15 of the second. Average B values for the complexes were calculated using CNS v0.9.²⁵ B values for PNMT:7:2 are 45 Å² (protein), 43 Å² (**2**), 51 Å² (**7**), and 41 Å² (water). The average B values for the PNMT:7:3 complex are 51 Å² (protein), 37 Å² (**3**), 46 Å² (**7**), and 41 Å² (water). For the purposes of comparison, the average B values for the PNMT:7:1 complex are 47 Å² (protein), 46 Å² (**1**), 50 Å² (**7**), and 46 Å² (water).

Root-mean-square deviations between pairs of structures and subunits were calculated using Insight II²⁷ (Table 3). ClogP values were calculated using the CLOGP module in SYBYL.³⁰ For comparison of inhibitor binding, the programs Insight II²⁷ and O²⁶ were used: crystal structures were first superimposed by least-squares analysis of all enzyme C α atoms, and then the position and orientation of each inhibitor within the active site were analyzed and compared. Distances between atoms were measured using O.²⁶ Figures of the enzyme reaction and active site interactions were created using ISIS.³¹ All other figures were generated using Molscript,³² Bobscript,³³ Insight II,²⁷ and O.²⁶

Inhibitor Modeling. Inhibitor models were built into their respective electron density maps based on the shape and contour of the electron density in the active site. Using the program O,²⁶ each inhibitor was rotated and translated to a number of orientations, until a fit with the electron density was achieved. Partial disorder is observed around the aliphatic ring of **2**, suggesting that this region of the inhibitor could be flexible when bound to the protein. Alternate binding modes were modeled to investigate whether better fits could be achieved between **2** and the electron density, but all other binding modes resulted in strong (3σ or higher) residual $F_o - F_c$ electron density. The final refined conformation of **2** was modeled using the strong density for the iodine atom and the density for the aromatic ring as a guide. Thus, the electron density around the iodine in Figure 3B is consistent with the scattering expected from an atom of this size. The position of the iodine was confirmed using high contour electron density maps. In addition, continuous electron density (at the 1σ level) between the modeled iodine atom and the side chain of Met258 (not shown) is indicative of strong van der Waals interactions between the two groups.

Molecular Modeling. The structures in Figures 6 and 7 were constructed using the SYBYL software suite.³⁰ The structure of **3** in Figure 7 was generated from the crystal

structure reported in this paper. The other structures were built in SYBYL and are shown as low-energy conformations from the "Compute: Minimize ..." function, using Gasteiger–Huckel charges. The structures were superimposed using both ends of a 2.0 Å normal through the centroids of the aromatic rings, and the lone pairs on the aliphatic ring nitrogens (2.4 Å long, to simulate hydrogen-bonding distance). Hydrogens have been omitted for clarity.

Acknowledgment. J.L.M. is the recipient of an Australian Research Council Senior Research Fellowship. This work was funded by the National Institutes of Health (HL34193), the University of Queensland Foundation, and the Australian Research Council.

References

- Gunne, L. M. Relative Adrenaline Content in Brain Tissue. *Acta Physiol. Scand.* **1962**, *56*, 324–333.
- Fuller, R. W. Pharmacology of Brain Epinephrine Neurons. *Annu. Rev. Pharmacol. Toxicol.* **1982**, *22*, 31–55.
- Martin, J. L.; Begun, J.; McLeish, M. J.; Caine, J. M.; Grunewald, G. L. Getting the Adrenaline Going: Crystal Structure of the Adrenaline-Synthesizing Enzyme PNMT. *Structure* **2001**, *9*, 977–985.
- Bondinell, W. E.; Chapin, F. W.; Frazee, J. S.; Girard, G. R.; Holden, K. G.; Kaiser, C.; Maryanoff, C.; Perchonock, C. D.; Gessner, G. W.; Hieble, J. P.; Hilleagass, L. M.; Pendleton, R. G.; Sawyer, J. L. Inhibitors of Phenylethanolamine *N*-Methyltransferase and Epinephrine Biosynthesis: A Potential Source of New Drugs. *Drug Metab. Rev.* **1983**, *14*, 709–721.
- Toomey, R. E.; Horng, J. S.; Hemrick-Luecke, S. K.; Fuller, R. W. α_2 -Adrenoreceptor Affinity of Some Inhibitors of Norepinephrine *N*-Methyltransferase. *Life Sci.* **1981**, *29*, 2467–2472.
- Goldstein, M.; Saito, M.; Lew, J. Y.; Hieble, J. P.; Pendleton, R. G. The Blockade of α_2 -Adrenoceptors by the PNMT Inhibitor SK&F 64139. *Eur. J. Pharmacol.* **1980**, *67*, 305–308.
- Grunewald, G. L.; Dahanukar, V. H.; Jalluri, R. K.; Criscione, K. R. Synthesis, Biochemical Evaluation, and Classical and Three-dimensional Quantitative Structure–activity Relationship Studies of 7-Substituted-1,2,3,4-tetrahydroisoquinolines and Their Relative Affinities Toward Phenylethanolamine *N*-Methyltransferase and the α_2 -Adrenoceptor. *J. Med. Chem.* **1999**, *42*, 118–134.
- Grunewald, G. L.; Dahanukar, V. H.; Criscione, K. R. Effects of a 3-Alkyl-, 4-Hydroxy- and/or 8-Aromatic-substituent on the Phenylethanolamine *N*-Methyltransferase Inhibitor Potency and α_2 -Adrenoceptor Affinity of 2,3,4,5-Tetrahydro-1*H*-2-benzazepines. *Bioorg. Med. Chem.* **2001**, *9*, 1957–1965.
- Pendleton, R. G.; Gessner, G.; Weiner, G.; Jenkins, B.; Sawyer, J.; Bondinell, W.; Intocchia, A. Studies on SK&F 29661, an Organ-specific Inhibitor of Phenylethanolamine *N*-Methyltransferase. *J. Pharmacol. Exp. Ther.* **1979**, *208*, 24–30.
- Grunewald, G. L.; Caldwell, T. M.; Li, Q.; Slavica, M.; Criscione, K. R.; Borchardt, R. T.; Wang, W. Synthesis and Biochemical Evaluation of 3-Fluoromethyl-1,2,3,4-tetrahydroisoquinolines as Selective Inhibitors of Phenylethanolamine *N*-Methyltransferase versus the α_2 -Adrenoceptor. *J. Med. Chem.* **1999**, *42*, 3588–3601.
- Grunewald, G. L.; Caldwell, T. M.; Dahanukar, V. H.; Jalluri, R. K.; Criscione, K. R. Comparative Molecular Field Analysis (CoMFA) Models of Phenylethanolamine *N*-Methyltransferase (PNMT) and the α_2 -Adrenoceptor: The Development of New, Highly Selective Inhibitors of PNMT. *Bioorg. Med. Chem. Lett.* **1999**, *9*, 481–486.
- Grunewald, G. L.; Dahanukar, V. H.; Caldwell, T. M.; Criscione, K. R. Examination of the Role of the Acidic Hydrogen in Imparting Selectivity of 7-(Aminosulfonyl)-1,2,3,4-tetrahydroisoquinoline (SK&F 29661) Toward Inhibition of Phenylethanolamine *N*-Methyltransferase vs the α_2 -Adrenoceptor. *J. Med. Chem.* **1997**, *40*, 3997–4005.
- Grunewald, G. L.; Dahanukar, V. H.; Ching, P.; Criscione, K. R. Effect of Ring Size or an Additional Heteroatom on the Potency and Selectivity of Bicyclic Benzylamine-Type Inhibitors of the Enzyme Phenylethanolamine *N*-Methyltransferase. *J. Med. Chem.* **1996**, *39*, 3539–3546.
- Grunewald, G. L.; Caldwell, T. M.; Li, O.; Dahanukar, V. H.; McNeil, B. Criscione, K. R. Enantiospecific Synthesis of 3-Fluoromethyl-, 3-Hydroxymethyl-, and 3-Chloromethyl-1,2,3,4-tetrahydroisoquinolines as Selective Inhibitors of Phenylethanolamine *N*-Methyltransferase versus the α_2 -Adrenoceptor. *J. Med. Chem.* **1999**, *42*, 4351–4361.
- Grunewald, G. L.; Skjaerbaek, N.; Monn, J. A. An Active Site Model of Phenylethanolamine *N*-Methyltransferase Using CoMFA. In *Trends in QSAR & Molecular Modelling 92*; Wermuth, C. G., Ed.; ESCOM Science Publishers B. V.: Leiden, 1993; pp 513–516.
- Ruggiero, D. A.; Cravo, S. L.; Golanov, E.; Gomez, R.; Anwar, M.; Reis, D. J. Adrenergic and Nonadrenergic Spinal Projections of a Cardiovascular-active Pressor Area of Medulla Oblongata: Quantitative Topographic Analysis. *Brain Res.* **1994**, *663*, 107–120.
- Hökfelt, T.; Fuxe, K.; Goldstein, M.; Johansson, O. Immunohistochemical Evidence for the Existence of Adrenaline Neurons in the Rat Brain. *Brain Res.* **1974**, *66*, 235–251.
- Crowley, W. R.; Terry, L. C.; Johnson, M. D. Evidence for the Involvement of Central Epinephrine Systems in the Regulation of Luteinizing Hormone, Prolactin, and Growth Hormone Release in Female Rats. *Endocrinology* **1982**, *110*, 1102–1107.
- Mefford, I. N.; Lister, R. G.; Ota, M.; Linnoila, M. Antagonism of Ethanol Intoxication in Rats by Inhibitors of Phenylethanolamine *N*-Methyltransferase. *Alcohol. Clin. Exp. Res.* **1990**, *14*, 53–57.
- Burke, W. J.; Chung, H. D.; Marshall, G. L.; Gillespie, K. N.; Joh, T. H. Evidence for Decreased Transport of PNMT Protein in Advanced Alzheimer's Disease. *J. Am. Geriatr. Soc.* **1990**, *38*, 1275–1282.
- Caine, J. M.; Macreadie, I. G.; Grunewald, G. L.; McLeish, M. J. Recombinant Human Phenylethanolamine *N*-Methyltransferase: Overproduction in *Escherichia coli*, Purification, and Characterization. *Protein Exp. Purif.* **1996**, *8*, 160–166.
- Grunewald, G. L.; Paradkar, V. M. A Regioselective Synthesis of 8,9-Dichloro-2,3,4,5-tetrahydro-1*H*-2-benzazepine (LY134046), a Potent Phenylethanolamine *N*-Methyltransferase Inhibitor. *Bioorg. Med. Chem. Lett.* **1991**, *1*, 59–60.
- Begun, J.; McLeish, M. J.; Caine, J. M.; Palant, E.; Grunewald, G. L.; Martin, J. L. Crystallization of PNMT, the Adrenaline-Synthesizing Enzyme, is Critically Dependent on a High Protein Concentration. *Acta Crystallogr. D Biol. Crystallogr.* **2002**, *58*, 314–315.
- Otwinkowski, Z.; Minor, W. Processing of X-ray Diffraction Data Collected in Oscillation Mode. *Methods Enzymol.* **1997**, *276*, 307–326.
- Brünger, A. T.; Adams, P. D.; Clore, G. M.; Delano, W. L.; Gros, P.; Grosse-Kuntzle, R. W.; Jiang, J. S.; Kuszewski, J.; Nilges, M.; Pamm, N. S.; Read, R. J.; Rice, L. M.; Simonson, T.; Warren, G. L. Crystallography & NMR System: A New Software Suite for Macromolecular Structure Determination. *Acta Crystallogr. D Biol. Crystallogr.* **1998**, *54*, 905–921.
- Jones, T. A.; Zou, J.-Y.; Cowan, S. W.; Kjeldgaard, M. Improved Methods for Building Protein Models in Electron Density Maps and the Location of Errors in These Models. *Acta Crystallogr. A* **1991**, *47*, 110–119.
- Accelrys Inc., Insight II Modeling Environment, Release 2000, San Diego, Accelrys Inc., 2001.
- Kleywegt, G. J.; Jones, T. A. Databases in Protein Crystallography. *Acta Crystallogr. D Biol. Crystallogr.* **1998**, *54*, 1119–1131.
- Brünger, A. T. Free R Value: A Novel Statistical Quantity for Assessing the Accuracy of Crystal Structures. *Nature* **1992**, *355*, 472–475.
- SYBYL 6.9; Tripos, Inc., 1699 South Hanley Rd., St. Louis, MO, 63144, USA.
- MDL Information Systems, Inc. *ISIS/DRAW*, version 2.3; MDL Information Systems, Inc., San Leandro, 2000.
- Kraulis, P. J. MOLSCRIPT: A Program to Produce Both Detailed and Schematic Plots of Protein Structures. *J. Appl. Crystallogr.* **1991**, *24*, 946–950.
- Esnouf, R. M. An Extensively Modified Version of MolScript that Includes Greatly Enhanced Colouring Capabilities. *J. Mol. Graph. Model.* **1997**, *15*, 132–134.
- Grunewald, G. L.; McLeish, M. J.; Criscione, K. R. Phenylethanolamine *N*-Methyltransferase Kinetics: Bovine versus Recombinant Human Enzyme. *Bioorg. Med. Chem. Lett.* **2001**, *11*, 1579–1582.
- Engh, R. A.; Huber, R. Accurate Bond Lengths and Angle Parameters for X-ray Protein Structure Refinement. *Acta Crystallogr. A* **1991**, *47*, 392–400.